nature biotechnology

LETTERS

https://doi.org/10.1038/s41587-019-0035-0

NFIA is a gliogenic switch enabling rapid derivation of functional human astrocytes from pluripotent stem cells

Jason Tchieu[1,2]*, Elizabeth L. Calder[1,2], Sudha R. Guttikonda[1,2,3], Eveline M. Gutzwiller[1,2], Kelly A. Aromolaran[4], Julius A. Steinbeck[1,2], Peter A. Goldstein[4] and Lorenz Studer[1,2]*

The mechanistic basis of gliogenesis, which occurs late in human development, is poorly understood. Here we identify nuclear factor IA (NFIA) as a molecular switch inducing human glial competency. Transient expression of NFIA is sufficient to trigger glial competency of human pluripotent stem cell-derived neural stem cells within 5 days and to convert these cells into astrocytes in the presence of glial-promoting factors, as compared to 3–6 months using current protocols. NFIA-induced astrocytes promote synaptogenesis, exhibit neuroprotective properties, display calcium transients in response to appropriate stimuli and engraft in the adult mouse brain. Differentiation involves rapid but reversible chromatin remodeling, glial fibrillary acidic protein (*GFAP*) promoter demethylation and a striking lengthening of the G1 cell cycle phase. Genetic or pharmacological manipulation of G1 length partially mimics NFIA function. We used the approach to generate astrocytes with region-specific or reactive features. Our study defines key mechanisms of the gliogenic switch and enables the rapid production of human astrocytes for disease modeling and regenerative medicine.

Astrocytes are the most abundant glial cell type in the human brain, and their dysfunction is a driver in the pathogenesis of both neurodevelopmental and neurodegenerative disorders[1]. The study of human astrocytes has proved challenging owing to their limited availability and regional heterogeneity[2]. Astrocytes are derived from late neural stem cells (NSCs). During early development, NSCs are fate-restricted to exclusively produce neurons, while at later stages they undergo a switch from neurogenic to gliogenic competency, resulting in progressive production of astrocytes and oligodendrocytes[3]. The molecular nature of the gliogenic switch has remained elusive, and its timing varies across species, from 7 days in the mouse to 6–9 months in humans[4]. These species-specific differences are reflected in methods for in vitro differentiation of pluripotent stem cells (PSCs), with the derivation of human astrocytes requiring 3–6 months[5,6]. Differentiation into NSCs results in a long neurogenic phase followed by a late gliogenic switch, mimicking the timeline of human glial development. Previous studies report the need to culture human PSC (hPSC)-derived NSCs for up to 24 weeks before obtaining large populations of functional astrocytes following differentiation[7,8]. Following extended culture, the gliogenic switch occurs spontaneously but the molecular mechanism underlying the switch remains unclear[9]. The protracted time for acquiring glial competency presents a roadblock in basic and translational studies of human astrocytes.

To monitor the period when astrocytes develop during hPSC differentiation, we generated a knock-in reporter line targeting the aquaporin-4 (AQP4) locus with a nuclear green fluorescent protein (H2B-GFP) (Supplementary Fig. 1). Previous strategies for generating astrocytes from hPSCs include the exposure of factors such as LIF, CNTF, BMP or serum to NSCs to trigger glial differentiation[10,11]. The onset of glial differentiation was moderately accelerated in NSCs treated with serum (Supplementary Fig. 2), and we tested whether such acceleration was correlated with changes in the expression of candidate factors including NFIA (Fig. 1a) previously implicated in glial fate acquistion[12–16].

To directly test whether these genes impact glial competency or differentiation, we used a homogeneous and stable neurogenic NSC population termed long-term human embryonic stem cell-derived neural stem cells (lt-hESNSCs[17], referred to as LTNSCs in this study). Unlike NSCs, LTNSCs do not spontaneously undergo the gliogenic switch following long-term culture but remain in the neurogenic phase[18] (Supplementary Fig. 3), making them ideal for identifying factors involved in the gliogenic switch. While knockdown of *LIN28B* did not show any obvious effect, overexpression of *NFIA* profoundly altered LTNSC morphology (Supplementary Fig. 4a,c) and correlated with expression of NFIA protein and CD44[19], a marker of glial competency, although it did not result in GFAP-positive cells (Fig. 1b). A subset of NFIA-expressing cells activated the *AQP4-H2B-GFP* reporter (Supplementary Fig. 4b). We hypothesized that overexpression of NFIA would trigger glial competency but block differentiation toward astrocytes. We performed a time course study in which LTNSCs were cultured in the presence (dox+) or absence (dox–) of NFIA expression. After 5 days, cells were switched to (dox–) either in a glial-promoting condition (+LIF) or in NSC maintenance medium (+epidermal growth factor/fibroblast growth factor 2 (EGF/FGF2)). Notably, continued expression of NFIA (dox+) prevented LTNSCs from expressing GFAP even in the presence of LIF (Fig. 1c (dox+)). In contrast, removal of doxycycline led to a decline in NFIA expression for both conditions, but GFAP expression was strongly induced only in the (+LIF) group and only after NFIA was sufficiently downregulated (Fig. 1c). We found that LIF was most efficient in generating GFAP-positive cells and in activating the AQP4-H2B-GFP reporter compared to other glial differentiation factors (Supplementary Fig. 5a,b). These results show that glial competency in neurogenic human NSCs can be achieved at as early as 5 days by transient expression of NFIA, compared with 90–180 days using current protocols (Supplementary Fig. 6a).

[1]The Center for Stem Cell Biology, New York, NY, USA. [2]Developmental Biology Program, Sloan-Kettering Institute for Cancer Research, New York, NY, USA. [3]Weill Cornell/Rockefeller/Sloan Kettering Tri-Institutional MD-PhD Program, New York, NY, USA. [4]Department of Anesthesiology, Weill Cornell Medicine, New York, NY, USA. *e-mail: tchieuj@mskcc.org; studerl@mskcc.org

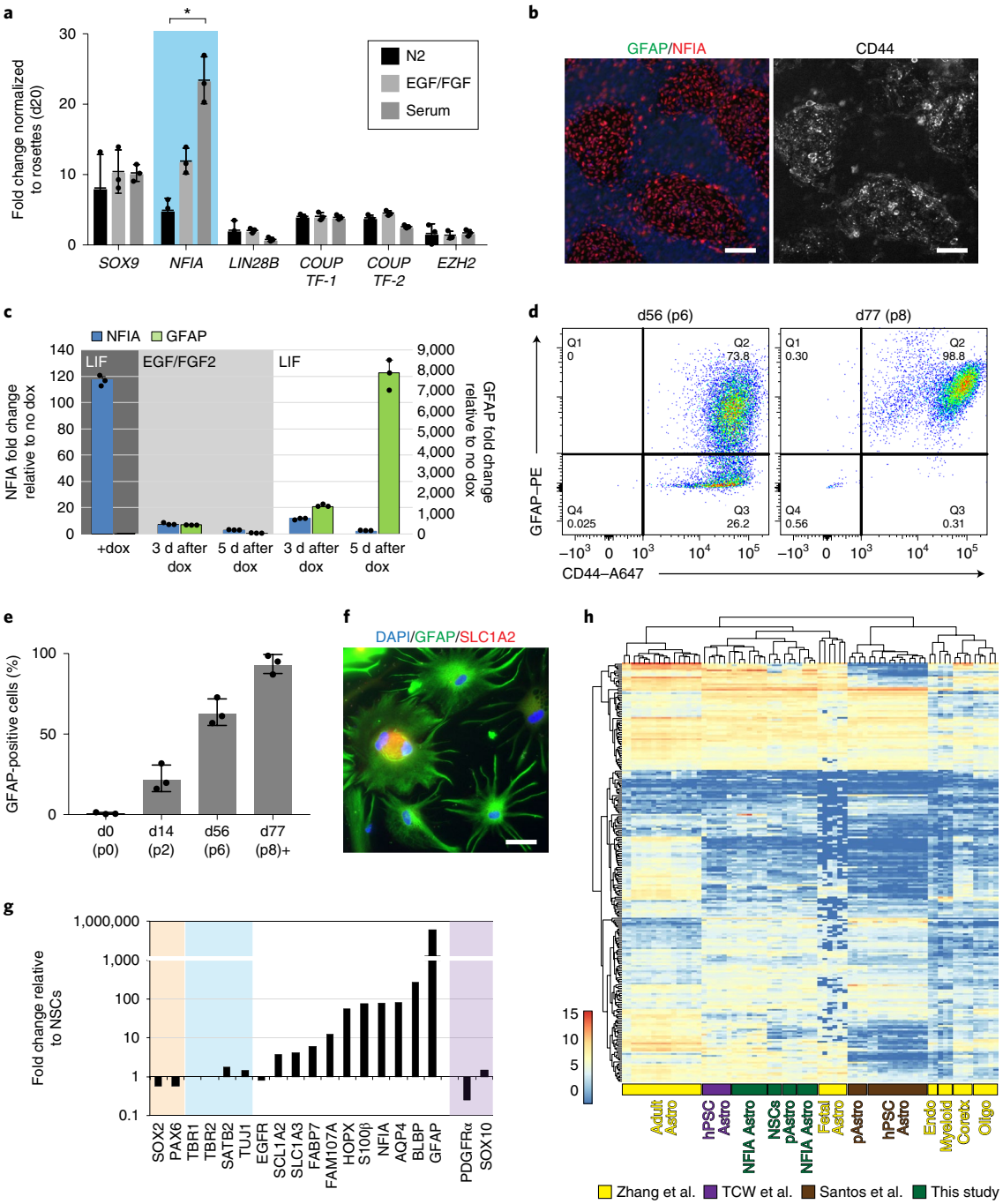

Fig. 1 | Transient expression of NFIA in neuroepithelial stem cells confers glial competency. a, Quantitative PCR of candidate genes associated with glial competency treated in serum (1% fetal bovine serum) conditions for 30 days. **One-way analysis of variance (ANOVA) ($P = 0.025$, $n = 3$ biologically independent experiments, mean values are represented by a black bar). **b**, Overexpression of NFIA leads to profound morphological changes within 5 days of doxycycline treatment ($n = 5$ biologically independent experiments). **c**, Quantitative PCR analysis of *GFAP* and *NFIA* expression in NSCs treated with doxycycline for 5 days and subsequent removal for an additional 3 and 5 days or continuous treatment (+dox) ($n = 3$ biologically independent experiments, mean values are represented in bar graph). **d**, Intracellular fluorescent activated cell sorter (FACS) analysis for GFAP and CD44 during the differentiation of NFIA-induced NSCs at 56 days (d56 p6) and 77 days (d77 p8) of culture. **e**, Quantification of the percentage of GFAP-expressing cells at different timepoints ($n = 3$ biologically independent experiments, mean values are represented in bar graph). **f**, Immunofluorescence staining of GFAP and SLC1A2 in d60 astrocyte culture ($n = 5$ biologically independent experiments). **g**, Quantitative PCR analysis of genes associated with NSCs, neurons, astrocytes and oligodendrocytes from NFIA-induced astrocytes. **h**, Heatmap of normalized read counts representing genes associated with astrocyte identity (Supplementary Table 1). Yellow, Zhang et al. [2]; purple, TCW et al.[6]; brown, Santos et al.[10]; green, this study. Scale bars, 50 µm. Error bars are calculated by s.e.m.

We determined the timing and efficiency of astrocyte generation using NFIA. While there was a robust increase in GFAP expression, not all cells were immediately immunoreactive to GFAP. We used intracellular fluorescent activated cell sorter to determine the absolute numbers of GFAP-positive and CD44-positive cells at different passages after NFIA induction (Supplementary Fig. 6b).

We achieved >60% GFAP-expressing cells by 56 days of culture (d56) and nearly 100% GFAP-positive cells after 77 days (d77) (Fig. 1d,e). We determined that the success of astrocyte generation was dependent on the transduction efficiency of the NFIA virus in NSCs. To further improve the efficiency of generating astrocytes from hPSCs (Supplementary Fig. 6c), we generated an inducible NFIA hPSC-line (NFIA-hPSC, Supplementary Fig. 7a). NFIA is not expressed in hPSCs and was induced by dox treatment to identify properly targeted clones (Supplementary Fig. 7b). Immunoblot analysis showed that NFIA levels were higher in the inducible line compared to transduced LTNSCs (Supplementary Fig. 7c).

To determine efficiency, we differentiated the inducible NFIA-hPSCs into cortical NSCs (Supplementary Fig. 6c) and induced NFIA for 10 days (Supplementary Fig. 7d,e). Over this time period, 65% of cells became CD44 positive. LIF treatment for 15 days led to 42% of cells expressing GFAP (Supplementary Fig. 7f–h). Immunostaining of the resulting cells showed expression of S100β and GFAP and loss of the proliferation marker KI-67 (Supplementary Fig. 7i). Finally, to test the suitability of the protocol for disease modeling, we differentiated isogenic control and patient-specific iPSCs harboring a mutation in the SOD1 gene (A4V)[20] toward cortical versus spinal cord progenitor identity[18,21] and confirmed their distinct antero-posterior marker expression (Supplementary Fig. 8a,b). By infecting the progenitors with NFIA, we observed the expression of GFAP-positive cells by 6–7 days of differentiation (Supplementary Fig. 8c) resulting in regionally distinct astrocytes (Supplementary Fig. 8d). This reaffirms that NFIA induction is a robust strategy for generation of astrocytes of specific regional identity across control and disease hPSCs.

The cells derived from NFIA-induced NSCs yielded astrocytes with complex morphology (Fig. 1f) that expressed a panel of genes representing astrocyte identity (Fig. 1g). To further determine whether NFIA-induced astrocytes matched those observed in vivo, we performed gene expression profiling (Fig. 1h). A broad set of RNA-sequencing data from NFIA-induced astrocytes at various stages of differentiation was compared to published datasets from hPSC-derived astrocytes from conventional, protracted differentiation conditions[6], hPSC-derived astrocytes from serum exposure[10] and those from primary human fetal tissue[22]. Initial comparison of the samples demonstrated high correlation between the NFIA-induced astrocytes and those generated using protracted methods. This is in contrast to hPSC-derived astrocytes using a serum-based method of differentiation (Supplementary Fig. 9a,b). We performed a comparative analysis of our dataset with one that encompasses freshly isolated fetal and adult astrocytes as well as a range of additional primary lineages isolated from human cortex[2] and across a set of astrocyte-specific genes shared among three independent astrocyte studies[23–25]. This analysis showed close correlation between NFIA-induced astrocytes and fetal astrocytes (Fig. 1h, Supplementary Fig. 9c,d and Supplementary Table 1).

We examined the functionality of NFIA-induced astrocytes. Astrocytes play critical roles during central nervous system development, including neuronal maturation[26], maintenance of metabolic homeostasis and regulation of inflammation[27]. Several genes associated with the formation of functional synapses[28] were upregulated (Supplementary Fig. 9e), suggesting that these cells exhibit functional properties in neuronal maturation. Immature neurons co-cultured in the presence of NFIA-induced astrocytes showed evidence of accelerated maturation by the increased expression and appearance of punctate SYN1 (synapsin-I) (Fig. 2a) and upregulation of an active zone marker MUNC13.1[29] (Fig. 2b). Additionally, the co-localization of pre- and postsynaptic markers, such as SYN1 and HOMER, indicated the formation of structural synapses (Fig. 2c and Supplementary Fig. 10). NFIA-induced astrocytes also promoted neuronal survival when subjected to glutamate excitotoxicity (Supplementary Fig. 11)[30]. Notably, following cytokine treatment, we could trigger the upregulation of reactive astrocyte (A1)-specific transcripts (Supplementary Fig. 12a,b) and complement (C3) secretion[1,31] (Fig. 2d). Morphologically, astrocytes cultured in different passages appeared to transition from large flat cells to cells with long and complex processes (Supplementary Fig. 13a).

NFIA-induced astrocytes can be stimulated to elicit calcium transients[32] in response to specific stimuli. Commercially available primary astrocytes isolated from human fetal brains (19–23 post-conception weeks) displayed morphology similar to NFIA-induced astrocytes; however, only a few cells responded to the stimuli (Supplementary Fig. 14g). In contrast, NFIA-induced astrocytes responded robustly to KCl and ATP (Fig. 2e and Supplementary Fig. 14a–d) with increasing ATP responsiveness over time (Supplementary Fig. 14h). When in co-culture with hPSC-derived neurons, NFIA-induced astrocytes adopted a more ramified appearance (Supplementary Fig. 13b), showed increased *AQP4-H2B-GFP* signal (Supplementary Fig. 14f) and the response to ATP increased twofold (Fig. 2g). In addition, the magnitude of the glutamate response was enhanced, suggesting a synergistic interaction between the two cell types in mutually driving both glial and neuronal maturation (Fig. 2f,g).

We tested whether NFIA-induced astrocytes would promote the functional maturation of immature hPSC-derived cortical neurons (Supplementary Fig. 15a). Whole-cell recordings from cortical neurons and cortical neurons cultured with NFIA-induced astrocytes revealed a resting membrane potential of -56.1 ± 2.5 and -72 ± 2.2 mV, respectively (Fig. 2h). Similarly, the input resistance of cortical neurons significantly decreased following co-culture with NFIA-induced astrocytes, further suggesting a more mature phenotype in the presence of astrocytes (Fig. 2i). To monitor the impact on synaptic maturation, we recorded basal spontaneous miniature excitatory postsynaptic currents (mEPSCs) (Supplementary Fig. 15b) and observed a decrease in inter-event interval (Supplementary Fig. 15c) and an increase in mEPSC frequency from 0.22 ± 0.01 to 0.39 ± 0.02 Hz (Fig. 2j) in neurons co-cultured with glia, indicating increased synaptic activity. We also observed an increase in amplitude (12.5 ± 0.2 versus 13.6 ± 0.2 pA) (Fig. 2k) and time course of decay (6.7 ± 0.3 versus 7.6 ± 0.3 ms) (Supplementary Fig. 15d) in mEPSCs from neurons in the presence of glia.

Finally, we transplanted neurogenic NSCs, NFIA-induced glial-competent NSCs or astrocytes in the adult mouse cortex and corpus callosum. At 2 weeks post-transplantation, the glial progenitors migrated extensively from the graft core along white matter tracts (Fig. 2l) whereas neurogenic NSCs resulted in a dense graft composed largely of neurons (Supplementary Fig. 16a–c). The grafted NFIA-induced cells maintained expression of both AQP4-H2B-GFP and GFAP, and displayed morphological features characteristic of human astrocytes by 6 weeks post-transplantation (Fig. 2m and Supplementary Fig. 16d–f), with complex morphologies and extensive GFAP-positive projections spanning multiple cortical regions[33] (Supplementary Fig. 16g).

The above in vitro and in vivo data demonstrate that transient NFIA expression generates functional, region-specific human astrocytes on demand at high speed and with efficiency. Furthermore, they show that NFIA is a key component of the molecular switch for triggering human glial competency. To explore the NFIA mechanism of action, we returned to our initial observation that transient NFIA expression triggers glial competency but does not induce endogenous NFIA expression (refer to Fig. 1c). Once doxycycline is removed and cells are maintained in NSC media, they lose glial competency (Fig. 3a) and return to a neurogenic state (Fig. 3b). We performed a time course analysis of ectopic NFIA expression followed by sorting for CD44-positive cells and replating in the absence of dox (dox–) (Fig. 3c). We confirmed that NFIA expression is lost after 3 days of culture without doxycycline (d9) (Fig. 3d). Based on gene expression data by RNA sequencing, we observed

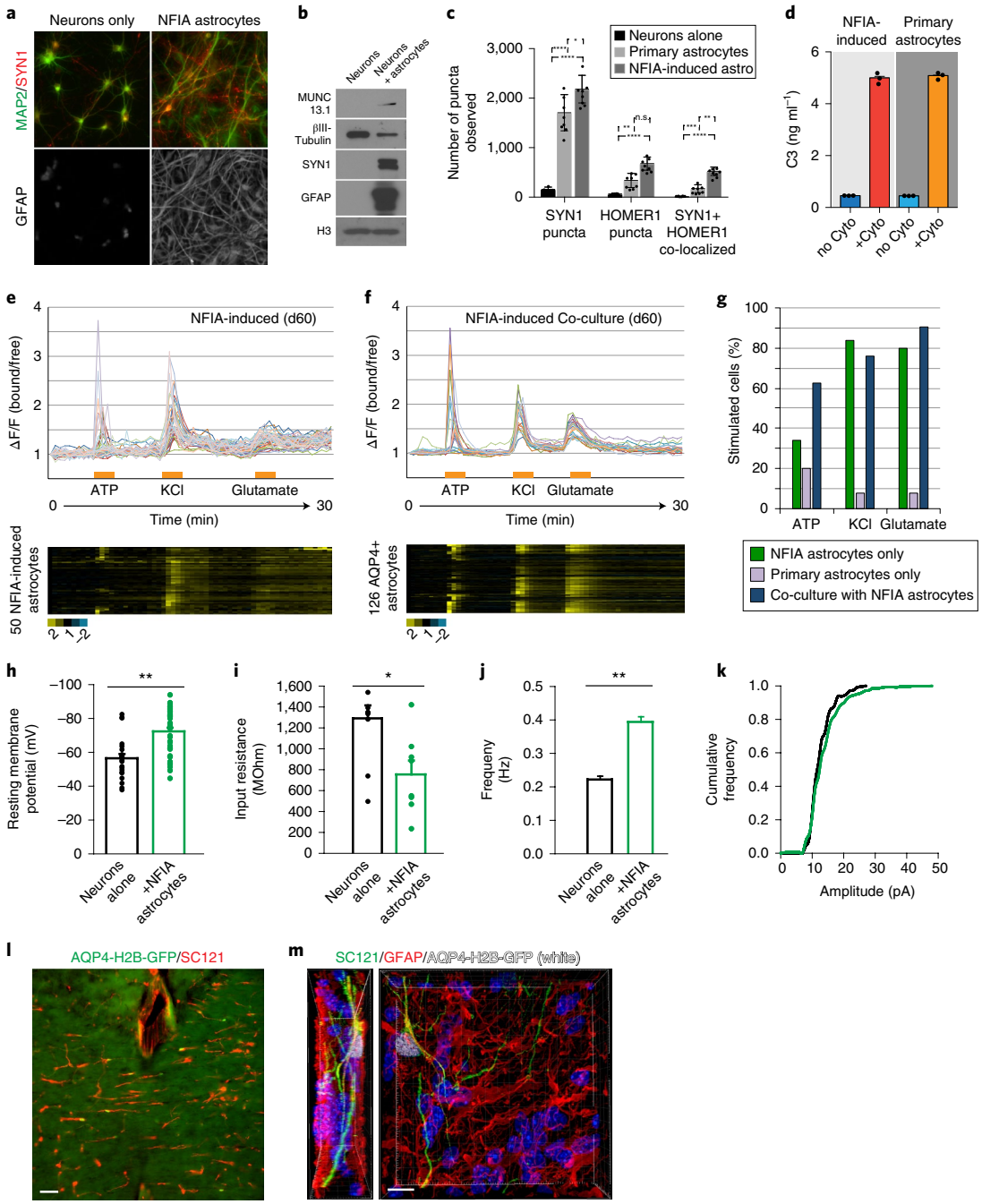

Fig. 2 | NFIA-induced astrocytes are functional. a, Immunofluorescence staining of MAP2 and synapsin-1 (SYN1) on neurons cultured with or without NFIA-induced astrocytes ($n=3$ biologically independent experiments). **b**, Immunoblot analysis of markers of maturity, MUNC13.1 and SYN1, in neurons cultured with or without astrocytes ($n=3$ biologically independent experiments). **c**, Bar chart representing the quantification of SYN1 and HOMER1 puncta on TUJ1-positive neurons ($n=8$ biologically independent experiments, mean values are represented in the bar graph) cultured with or without astrocytes for 28 days. One-way ANOVA *($P<0.05$), **($P<0.01$), ****($P<0.001$). **d**, Bar chart representing the amount of complement (C3) released from NFIA-induced or primary astrocytes treated with IL1α, tumor necrosis factor and C1q for 24 h ($n=3$ biologically independent experiments, mean values are presented in bar graph). **e**, Ratiometric plots of purified NFIA-induced astrocytes (60 days) incubated with the Fura-2 calcium dye and stimulated with adenosine triphosphate (ATP), potassium chlorate (KCl) and glutamate. All data points are plotted as a heatmap below. **f**, Ratiometric plots of NFIA-induced astrocytes co-cultured with neurons incubated with Fura-2 calcium dye and stimulated with ATP, KCl and glutamate. Ratios were calculated on GFP-positive nuclei. All data points are plotted as a heatmap below. **g**, Quantification of the number of astrocytes responding to ATP, KCl or glutamate from data presented in **e**,**f** and Supplementary Fig. 13. **h**, Quantification of resting membrane potential. Student's *t*-test $P=0.0000186$, $n=23, 39$. **i**, Quantification of mean input resistance. Student's *t*-test $P=0.010$, $n=10, 8$. **j**, Mean frequency of neurons with or without astrocytes. Mann–Whitney rank sum $P=0.000155$. **k**, Cumulative distribution of all mEPSC amplitudes recorded. For control neurons 341 mEPSCs were recorded from ten neurons and, for neurons in the presence of glia, 629 mEPSCs were recorded from six neurons. All electrophysiology was performed on three biologically independent experiments. **l**, Immunofluorescence of NFIA-induced glial progenitors transplanted into mouse cortex depicts migration through the corpus callosum ($n=3$ biologically independent animals). Scale bar, 50 µm. **m**, Immunofluorescence of NFIA-induced astrocytes demonstrates co-expression of AQP4-H2B-GFP, GFAP and the human-specific marker SC-121 ($n=3$ biologically independent animals). Scale bar, 10 µm.

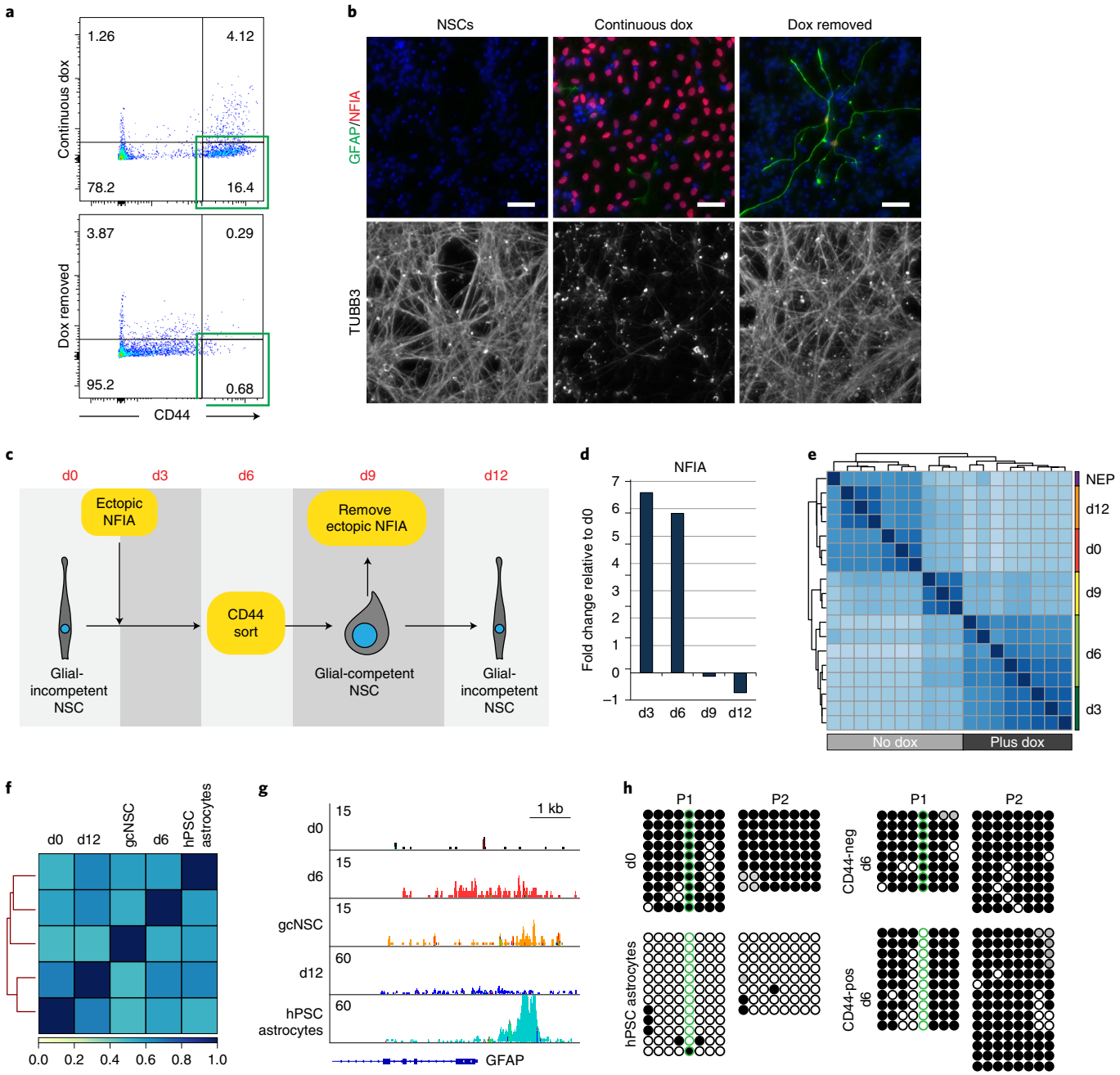

Fig. 3 | NFIA cannot maintain the glial-competent state. a, FACS plot of CD44-expressing cells treated with continuous doxycycline, or doxycycline removed, demonstrates that CD44 expression is lost after doxycycline removal. **b**, Immunofluorescence staining for NFIA, GFAP and TUBB3 in NSCs, NFIA-induced NSCs and NFIA-induced NSCs with doxycycline removal ($n = 3$ biologically independent experiments). **c**, Schematic representation of cells induced with NFIA and attaining glial competency followed by reversal to glial incompetency with doxycycline withdrawal. **d**, Quantitative PCR data of *NFIA* expression. **e**, Sample distance plot for RNA expression of NSCs at different timepoints related C. **f**, Sample distance plot for chromatin accessibility compared to glial-competent NSCs (gcNSCs) and hPSC-derived astrocytes (200 days of in vitro culture). **g**, Example assay for transposase-accessible chromatin using sequencing (ATAC-seq) tracks at the *GFAP* locus depicting the lack of chromatin accessibility in several NSC samples. **h**, Bisulfite sequencing of the promoter region of the *GFAP* promoter (P1 and P2) suggests that CD44-positive cells resulting from overexpression of NFIA leads to demethylation of a specific CpG on the *GFAP* promoter (green circles).

three major clusters among the samples throughout the time course (Fig. 3e and Supplementary Table 2). Of these, neuroepithelial-stage NSCs, LTNSCs (d0) and samples reverted to dox– clustered together, supporting the notion that the NFIA pulse cannot maintain glial competency following NFIA withdrawal.

Notably, NFIA expression for 6 days induced a chromatin accessibility landscape similar to that of hPSC-derived astrocytes (d200) or glial-competent NSCs (d80) (Fig. 3f). Differential chromatin accessibility was associated with a clear shift in the enrichment of transcription factor-binding motifs. *SOX* and *ZNF354C* motifs were enriched in the d0 (dox–) and the d12 (reverse) conditions, and *AP-1*, *NFIX* and *NFI* half-site motifs were highly enriched in the d6 (dox+) and astrocyte conditions (Supplementary Fig. 17). Unexpectedly, the *GFAP* promoter did not show differential

accessibility (Fig. 3g, bottom), even though our previous experiments showed robust induction of *GFAP* in the presence of LIF after only a short pulse of *NFIA* but not with LIF treatment alone. However, bisulfite sequencing of the GFAP promoter consistently highlighted one CpG in the *GFAP* promoter with a loss of methylation in CD44-positive cells (Fig. 3h) and was similarly unmethylated in astrocytes but not in LTNSCs. This CpG matches a *STAT3* binding site[34] that is predicted to inhibit STAT3 binding when methylated. These data suggest that NFIA induces glial competency by multiple modes, including the regulation of chromatin accessibility and DNA demethylation.

We examined the differential gene expression programs induced by NFIA overexpression and following NFIA withdrawal in LTNSCs using RNA sequencing and the functional annotation analysis software: Database for Annotation, Visualization, and Integrated Discovery (DAVID)[35]. Hierarchical clustering of all differentially expressed genes during the time course displayed three major clusters with distinct temporal profiles (Fig. 4a, labeled I, II and III). Cluster I includes genes associated with glial differentiation (Supplementary Fig. 18a). Genes associated with oligodendrocyte differentiation were absent from Cluster I. Cluster II comprises genes directly affected by *NFIA* expression that are rapidly lost following *NFIA* reduction (Supplementary Fig. 18b). Cluster III encompasses genes downregulated following expression of *NFIA*. These genes were specifically enriched for cell cycle-related processes, such as cell division, chromosome segregation, DNA repair and replication (Fig. 4b). *NFIA* triggered a negative regulation of cell cycle-specific genes (Fig. 4c), which was reversed after *NFIA* removal (Fig. 4d and Supplementary Fig. 19a).

We studied whether functional changes in cell cycle progression were the key to acquisition of glial competency. A large proportion of cells accumulated in G1 following *NFIA* expression in LTNSCs (Fig. 4e). Although expression of *CCNA1* was upregulated with NFIA (Supplementary Fig. 19b), there was a striking decrease in CCNA1 protein and marked increase in CDKN1A (p21) (Fig. 4f). Progressive lengthening of G1 was reported as a characteristic feature of the developing rodent cortex[36] from early embryonic (neurogenic) to later fetal (gliogenic) stages—a transition during which hPSC-derived NSCs showed progressive endogenous expression of NFIA (Supplementary Fig. 20a). To directly measure cell cycle lengthening, we used the FUCCI-O vector to determine the time spent by cells in G1[37]. Time-lapse analysis demonstrated that a large proportion of cells showed lengthening of the G1 phase in the (dox+) condition compared to uninduced cells (Supplementary Movies 1,x 2 and Supplementary Fig. 20b). We also explored whether reduction of *NFIA* levels would result in a more moderate G1 length compatible with acquiring glial fate. Indeed, when we titrated *NFIA* levels by varying dox concentrations, the percentage of cells in G1 gradually decreased along with reduced dox levels, and *GFAP* expression was induced only at lower dox concentrations in the presence of LIF (Supplementary Fig. 20d,e).

To examine whether pharmacological modulation of the cell cycle in the absence of NFIA expression is sufficient to trigger the gliogenic switch, we treated cells with olomoucine (Olo), a small molecule known to lengthen G1 timing in vitro[38]. Treatment of LTNSCs with Olo increased the percentage of cells in G1 (Supplementary Fig. 21a) but did not immediately activate expression of glial competency genes (Supplementary Fig. 21b). However, when Olo-treated LTNSCs were either maintained or induced to differentiate for an additional 12 days, we detected increased expression of glial competency genes and GFAP-positive cells (Supplementary Fig. 21c,d). Conversely, we knocked down *FZR1*(*CDH1*), which shortens the G1 cell cycle phase[39,40]. Short hairpin RNA (shRNA) constructs targeting *FZR1* showed efficient knockdown of the transcript (Fig. 4g), did not affect levels of NFIA expression and decreased the percentage of cells in G1 (Fig. 4h). Indeed, the knockdown of *FZR1* partially prevented NFIA-mediated induction of *CD44* and *GFAP* expression (Fig. 4i,j).

Finally, we explored the identity of candidate upstream activators of *NFIA*. Transforming growth factor beta (TGFβ) signaling has been implicated in timing of cell fate decisions in the spinal cord[41] and is known to modulate G1 arrest[42]. TGFβ1 treatment of neurogenic NSCs induced the expression of NFIA (Fig. 4k) and enrichment for cells in the G1 phase of the cell cycle (Fig. 4l). We treated neurogenic NSCs with TGFβ1 followed by culture in LIF-containing medium for 2 weeks, which resulted in the appearance of GFAP+ cells (Fig. 4m). These results indicate that TGFβ1-mediated induction of NFIA and concomitant G1 lengthening are sufficient to trigger gliogenesis. However, the resulting levels of NFIA expression, speed and efficiency did not match the results obtained with ectopic NFIA expression, suggesting that further investigation into additional extrinsic factors is required to fully substitute for forced NFIA expression.

While it has become routine to model neurodevelopmental or neurodegenerative diseases[43,44] with hPSC-derived neurons, the use of hPSC-derived astrocytes in such studies has remained limited[7,45]. This is due, in part, to the extremely protracted onset of the gliogenic switch in humans as compared to rodent cells, which is recapitulated in vitro and makes such studies laborious, costly and inefficient. Our work presents a simple, effective strategy based on the use of a single factor to drive glial competency and astrocyte differentiation (Fig. 4n). Our ability to combine overexpression of *NFIA* with patterning of early-stage NSCs enables the rapid derivation of region-specific astrocytes and will be of particular interest in studying the contribution of astrocytes to disorders affecting distinct brain regions, such as in Parkinson's disease, Alzheimer's

Fig. 4 | NFIA expression leads to a slower G1 cell cycle phase to induce glial competency. a, Unbiased hierarchical clustering of genes during the time course with three major clusters highlighted (Supplementary Table 2). **b**, Gene ontology analysis of the major biological processes from each cluster represented in **a**. **c**, Global analysis of all genes and genes specifically in the cell cycle ontology ($P < 0.000001$ calculated using hypergeometric distribution ($n =$ minimum of 3 biologically independent sequencing experiments). **d**, Graph of expression dynamics for all cell division cycle genes during the time course. **e**, Cell cycle analysis by FACS on NSCs with or without dox for 7 days ($n = 12$ biologically independent experiments). One-sided paired *t*-test on the G1 population with $^{****}P < 0.0001$). **f**, Immunoblot analysis of CCNA1 and CDKN1A in LTNSCs with or without dox for 7 days ($n = 3$ biologically independent experiments). **g**, Quantitative PCR assessing the knockdown efficiency of shFZR1 in the presence of *NFIA* overexpression (one-way ANOVA, $^{***}P < 0.0004$, $^{*}P < 0.0185$, $n = 3$ biological independent experiments). **h**, Analysis of the cell cycle phase with or without shRNA to FZR1. One-sided paired *t*-test on the S phase population with $P < 0.07$ (ns), $n = 3$ biological independent experiments. **i**, Quantitative PCR analysis of *CD44* expression in *NFIA*-induced cells with or without shFZR1 (one-way ANOVA, $^{**}P = 0.0055$, $n = 3$ biological independent experiments). **j**, Quantitative PCR analysis of *GFAP* expression in *NFIA*-induced cells similar to **I** but further induced with LIF (one-way ANOVA, $^{**}P = 0.001$, $n = 3$ biologically independent experiments). **k**, Immunoblot analysis of NFIA when induced with various levels of TGFβ1 for 7 days ($n = 3$ biologically independent experiments). **l**, Cell cycle analysis by FACS on NSCs treated with or without TGFβ1 for 48 h ($n = 3$ biologically independent experiments). One-sided paired *t*-test on the G1 cell cycle phase with $^{*}P = 0.0386$. **m**, Immunofluorescence staining for NFIA and GFAP on cultures treated with or without TGFβ1 for 14 days ($n = 3$ biologically independent experiments). **n**, Immunofluorescence staining for CD44 on cultures treated with or without TGFβ1 for 16 days ($n = 3$ biologically independent experiments). **o**, Model of NFIA-induced glial competency. Scale bars, 50 μm.

disease or amyotrophic lateral sclerosis. Such region-specific astrocytes can be further harnessed for the study of distinct trophic support, as reported for primary astrocytes derived from discrete brain regions[46,47].

One potential concern in using *NFIA* to fast-forward human neural development is whether the resulting cell types match bona fide, in vivo–derived astrocytes or represent an artifactual in vitro cell type. We demonstrate faithful transcriptional identity and robust functional features of NFIA-induced astrocytes, including calcium responses to relevant stimuli that not only match but exceed the performance of primary human fetal astrocytes. In addition, we show that NFIA-induced astrocytes reliably induce maturation of hPSC-derived neurons, a functional property commonly associated with mature, adult-like astrocytes[2]. Therefore, the NFIA protocol yields astrocyte populations highly relevant for human molecular, physiological and disease-related studies.

Contrary to the role of NFIA overexpression in promoting competency for astrocyte differentiation, NFIA, when expressed at high levels, prevents further differentiation into astrocytes unless it is downregulated. We presume this is partially due to high levels of NFIA leading to G1 cell cycle arrest. It is possible that this finding explains the low efficiency of astrocyte induction in

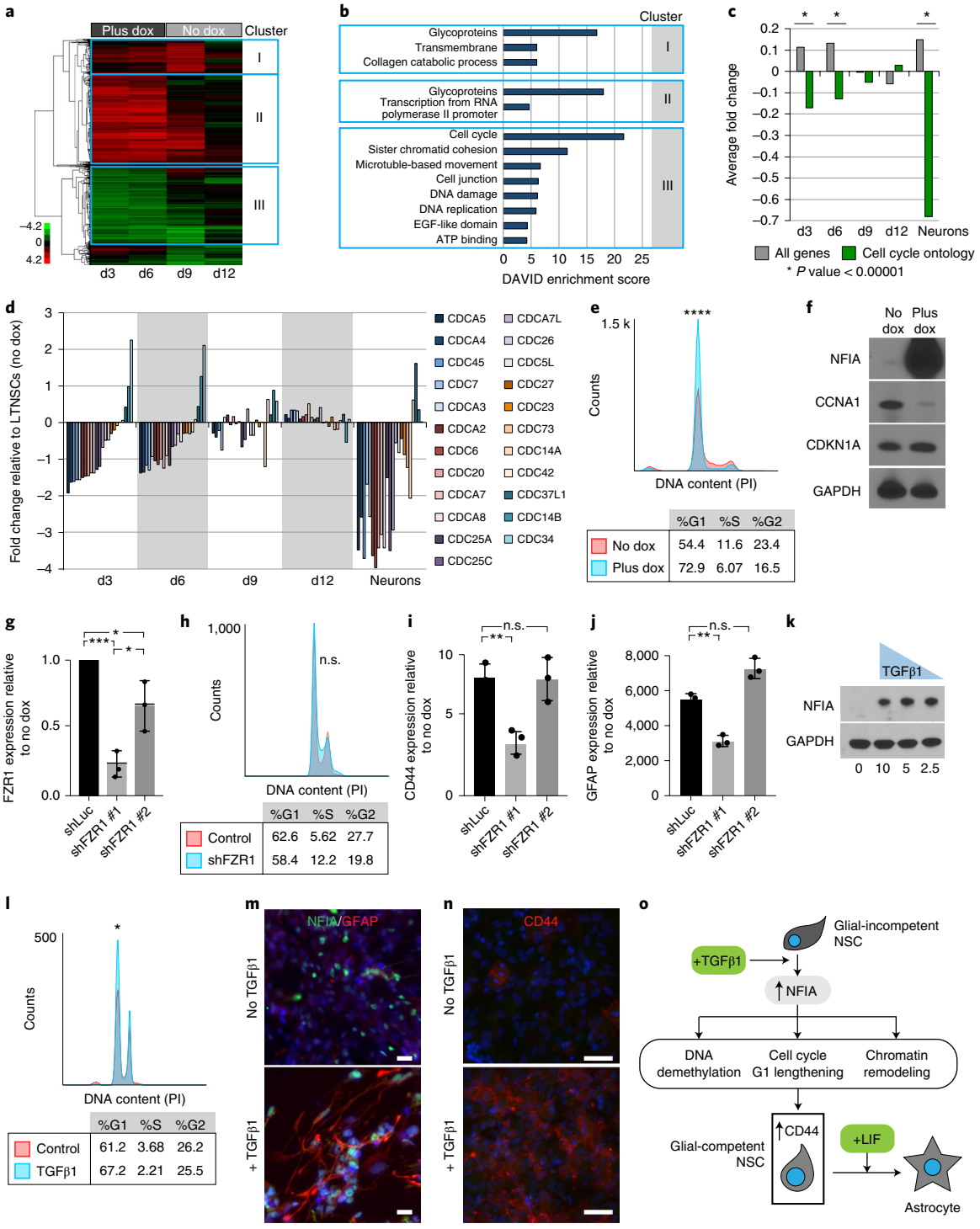

previous ectopic expression studies in the chicken spinal cord[13], and that *NFIA* levels need to be carefully titrated or followed by *NFIA* withdrawal to achieve optimal results. *NFIA* null mutant mice show a near complete loss of GFAP expression in the adult brain[48]. A similar phenotype is observed in nuclear factor 1B (*NFIB*) mutant mice[49]. The probable redundancy of *NFIA* and *NFIB* in vivo may explain why single mutant mice do not exhibit a more severe early developmental glial specification phenotype[3]. Further exploration of the interaction among TGFβ, NFIA/B and other factors in establishing the coordinated modulation of the cell cycle that promotes glial competency during in vivo development will be of particular interest. Another intriguing finding is that transient overexpression of *NFIA* is not sufficient to activate an irreversible, endogenous glial competency program in the absence of STAT or BMP signal activators. These results indicate that *NFIA* may act in concert with other factors such as *SOX9* to further stabilize the gliogenic program[50].

Our mechanistic studies demonstrate that *NFIA* can rapidly trigger a chromatin state similar to that of astrocytes. The gene expression data reveal that *NFIA* induces transcription of a broad set of genes related to glial specification. Following release of *NFIA* overexpression, several genes associated with astrocyte identity remain upregulated for at least 3 days, suggesting that *NFIA* may open the chromatin landscape at these particular genes to poise them for activation in response to extrinsic factors. We found the NFI– motif to be highly enriched in the accessible chromatin with *NFIA* expression. Other highly enriched motifs, such as AP-1/JunB, require further study of their potential role ineither astrocyte differentiation or the maintenance of glial competency. The role of NFIA as a negative cell cycle regulator was recapitulated in part by pharmacological or genetic modulation of the G1 phase. The role of the cell cycle in modulating cell fate decisions in undifferentiated hPSC populations has been described previously[51]. Our data demonstrate that NFIA expression lengthens G1, and that high NFIA levels trigger G1 arrest. Further exploration of the interaction among TGFβ, NFIA and other factors in establishing the coordinated, progressive modulation of the cell cycle that promotes the glial-competent state during development will be of particular interest.

Online content

Any methods, additional references, Nature Research reporting summaries, source data, statements of data availability and associated accession codes are available at https://doi.org/10.1038/s41587-019-0035-0.

Received: 21 March 2018; Accepted: 11 January 2019;
Published online: 25 February 2019

References

1. Liddelow, S. A. et al. Neurotoxic reactive astrocytes are induced by activated microglia. *Nature* **541**, 481–487 (2017).
2. Zhang, Y. et al. Purification and characterization of progenitor and mature human astrocytes reveals transcriptional and functional differences with mouse. *Neuron* **89**, 37–53 (2016).
3. Molofsky, A. V. et al. Astrocytes and disease: a neurodevelopmental perspective. *Genes Dev.* **26**, 891–907 (2012).
4. Sauvageot, C. M. & Stiles, C. D. Molecular mechanisms controlling cortical gliogenesis. *Curr. Opin. Neurobiol.* **12**, 244–249 (2002).
5. Studer, L., Vera, E. & Cornacchia, D. Programming and reprogramming cellular age in the era of induced pluripotency. *Cell Stem Cell* **16**, 591–600 (2015).
6. Tcw, J. et al. An efficient platform for astrocyte differentiation from human induced pluripotent stem cells. *Stem Cell Reports* **9**, 600–614 (2017).
7. Krencik, R. et al. Dysregulation of astrocyte extracellular signaling in Costello syndrome. *Sci. Transl. Med.* **7**, 286ra266 (2015).
8. Tao, Y. & Zhang, S. C. Neural subtype specification from human pluripotent stem cells. *Cell Stem Cell* **19**, 573–586 (2016).
9. Chandrasekaran, A., Avci, H. X., Leist, M., Kobolak, J. & Dinnyes, A. Astrocyte differentiation of human pluripotent stem cells: new tools for neurological disorder research. *Front. Cell. Neurosci.* **10**, 215 (2016).
10. Santos, R. et al. Differentiation of inflammation-responsive astrocytes from glial progenitors generated from human induced pluripotent stem cells. *Stem Cell Reports* **8**, 1757–1769 (2017).
11. Krencik, R., Weick, J. P., Liu, Y., Zhang, Z. J. & Zhang, S. C. Specification of transplantable astroglial subtypes from human pluripotent stem cells. *Nat. Biotechnol.* **29**, 528–534 (2011).
12. Stolt, C. C. et al. The Sox9 transcription factor determines glial fate choice in the developing spinal cord. *Genes Dev.* **17**, 1677–1689 (2003).
13. Deneen, B. et al. The transcription factor NFIA controls the onset of gliogenesis in the developing spinal cord. *Neuron* **52**, 953–968 (2006).
14. Patterson, M. et al. let-7 miRNAs can act through notch to regulate human gliogenesis. *Stem Cell Reports* **3**, 758–773 (2014).
15. Naka, H., Nakamura, S., Shimazaki, T. & Okano, H. Requirement for COUP-TFI and II in the temporal specification of neural stem cells in CNS development. *Nat. Neurosci.* **11**, 1014–1023 (2008).
16. Hirabayashi, Y. et al. Polycomb limits the neurogenic competence of neural precursor cells to promote astrogenic fate transition. *Neuron* **63**, 600–613 (2009).
17. Koch, P., Opitz, T., Steinbeck, J. A., Ladewig, J. & Brustle, O. A rosette-type, self-renewing human ES cell-derived neural stem cell with potential for in vitro instruction and synaptic integration. *Proc. Natl Acad. Sci. USA* **106**, 3225–3230 (2009).
18. Elkabetz, Y. et al. Human ES cell-derived neural rosettes reveal a functionally distinct early neural stem cell stage. *Genes Dev.* **22**, 152–165 (2008).
19. Liu, Y. et al. CD44 expression identifies astrocyte-restricted precursor cells. *Dev. Biol.* **276**, 31–46 (2004).
20. Chen, H. et al. Modeling ALS with iPSCs reveals that mutant SOD1 misregulates neurofilament balance in motor neurons. *Cell Stem Cell* **14**, 796–809 (2014).
21. Calder, E. L. et al. Retinoic acid-mediated regulation of GLI3 enables efficient motoneuron derivation from human ESCs in the absence of extrinsic SHH activation. *J. Neurosci.* **35**, 11462–11481 (2015).
22. Magistri, M. et al. A comparative transcriptomic analysis of astrocytes differentiation from human neural progenitor cells. *Eur. J. Neurosci.* **44**, 2858–2870 (2016).
23. Lovatt, D. et al. The transcriptome and metabolic gene signature of protoplasmic astrocytes in the adult murine cortex. *J. Neurosci.* **27**, 12255–12266 (2007).
24. Cahoy, J. D. et al. A transcriptome database for astrocytes, neurons, and oligodendrocytes: a new resource for understanding brain development and function. *J. Neurosci.* **28**, 264–278 (2008).
25. Doyle, J. P. et al. Application of a translational profiling approach for the comparative analysis of CNS cell types. *Cell* **135**, 749–762 (2008).
26. Ullian, E. M., Sapperstein, S. K., Christopherson, K. S. & Barres, B. A. Control of synapse number by glia. *Science* **291**, 657–661 (2001).
27. Sofroniew, M. V. Astrocyte barriers to neurotoxic inflammation. *Nat. Rev. Neurosci.* **16**, 249–263 (2015).
28. Allen, N. J. & Eroglu, C. Cell biology of astrocyte-synapse interactions. *Neuron* **96**, 697–708 (2017).
29. Betz, A. et al. Munc13-1 is a presynaptic phorbol ester receptor that enhances neurotransmitter release. *Neuron* **21**, 123–136 (1998).
30. Sofroniew, M. V. & Vinters, H. V. Astrocytes: biology and pathology. *Acta Neuropathol.* **119**, 7–35 (2010).
31. Liddelow, S. A. & Barres, B. A. Reactive astrocytes: production, function, and therapeutic potential. *Immunity* **46**, 957–967 (2017).
32. Cornell-Bell, A. H., Finkbeiner, S. M., Cooper, M. S. & Smith, S. J. Glutamate induces calcium waves in cultured astrocytes: long-range glial signaling. *Science* **247**, 470–473 (1990).
33. Oberheim, N. A. et al. Uniquely hominid features of adult human astrocytes. *J. Neurosci.* **29**, 3276–3287 (2009).
34. Rajan, P. & McKay, R. D. Multiple routes to astrocytic differentiation in the CNS. *J. Neurosci.* **18**, 3620–3629 (1998).
35. Huang da, W., Sherman, B. T. & Lempicki, R. A. Systematic and integrative analysis of large gene lists using DAVID bioinformatics resources. *Nat. Protoc.* **4**, 44–57 (2009).
36. Takahashi, T., Nowakowski, R. S. & Caviness, V. S. Jr. The cell cycle of the pseudostratified ventricular epithelium of the embryonic murine cerebral wall. *J. Neurosci.* **15**, 6046–6057 (1995).
37. Sakaue-Sawano, A. et al. Visualizing spatiotemporal dynamics of multicellular cell-cycle progression. *Cell* **132**, 487–498 (2008).
38. Calegari, F. & Huttner, W. B. An inhibition of cyclin-dependent kinases that lengthens, but does not arrest, neuroepithelial cell cycle induces premature neurogenesis. *J. Cell. Sci.* **116**, 4947–4955 (2003).
39. Vodermaier, H. C. APC/C and SCF: controlling each other and the cell cycle. *Curr. Biol.* **14**, R787–R796 (2004).
40. Sigl, R. et al. Loss of the mammalian APC/C activator FZR1 shortens G1 and lengthens S phase but has little effect on exit from mitosis. *J. Cell. Sci.* **122**, 4208–4217 (2009).

41. Garcia-Campmany, L. & Marti, E. The TGFbeta intracellular effector Smad3 regulates neuronal differentiation and cell fate specification in the developing spinal cord. *Development* **134**, 65–75 (2007).
42. Zhang, Y., Alexander, P. B. & Wang, X. F. TGF-beta family signaling in the control of cell proliferation and survival. *Cold Spring Harb Perspect Biol* **9**, a022145 (2017).
43. Zeltner, N. & Studer, L. Pluripotent stem cell-based disease modeling: current hurdles and future promise. *Curr. Opin. Cell Biol.* **37**, 102–110 (2015).
44. Sances, S. et al. Modeling ALS with motor neurons derived from human induced pluripotent stem cells. *Nat. Neurosci.* **19**, 542–553 (2016).
45. Williams, E. C. et al. Mutant astrocytes differentiated from Rett syndrome patients-specific iPSCs have adverse effects on wild-type neurons. *Hum. Mol. Genet.* **23**, 2968–2980 (2014).
46. Le Roux, P. D. & Reh, T. A. Astroglia demonstrate regional differences in their ability to maintain primary dendritic outgrowth from mouse cortical neurons in vitro. *J. Neurobiol.* **27**, 97–112 (1995).
47. Holmqvist, S. et al. Generation of human pluripotent stem cell reporter lines for the isolation of and reporting on astrocytes generated from ventral midbrain and ventral spinal cord neural progenitors. *Stem Cell Res.* **15**, 203–220 (2015).
48. das Neves, L. et al. Disruption of the murine nuclear factor I-A gene (Nfia) results in perinatal lethality, hydrocephalus, and agenesis of the corpus callosum. *Proc. Natl Acad. Sci. USA* **96**, 11946–11951 (1999).
49. Steele-Perkins, G. et al. The transcription factor gene Nfib is essential for both lung maturation and brain development. *Mol. Cell. Biol.* **25**, 685–698 (2005).
50. Canals, I. et al. Rapid and efficient induction of functional astrocytes from human pluripotent stem cells. *Nat. Methods* **15**, 693–696 (2018).
51. Pauklin, S. & Vallier, L. The cell-cycle state of stem cells determines cell fate propensity. *Cell* **155**, 135–147 (2013).

Acknowledgements

We are grateful to the members the Studer laboratory for helpful discussions and support for this project, and to G. Cederquist, M. Tomishima, S. Irion and V. Tabar for their critical comments on the manuscript. We would also like to give special thanks to A. Koff (MSKCC) for his helpful comments, experimental discussions regarding the cell cycle and comments on the manuscript. Additionally, we would like to thank A. Viale at Integrated Genomics Operation Core (MSKCC) for the RNA-sequencing studies, M. Witkin at the Epigenetics Core (MSKCC) for the ATAC sequencing, S. Fujisawa, E. Feng and V. Boyko at the Molecular Cytology Core (MSKCC) for help in calcium imaging studies and quantification of synaptic proteins, R. Garripa and H. Liu at the RNAi Core (MSKCC) for help with short hairpin RNA design and the Flow Cytometry Core (MSKCC) for the cell-sorting applications. J.T. was supported by the Tri-I Starr Stem Cell Scholars postdoctoral training fellowship. S.R.G was supported by the Ruth L. Kirschstein Individual Predoctoral NRSA for MD/PhD Fellowship (No. 1F30MH115616-01) and by a Medical Scientist Training Program grant from the National Institute of General Medical Sciences of the National Institutes of Health (No. T32GM007739) to the Weill Cornell/Rockefeller/Sloan Kettering Tri-Institutional MD-PhD Program. E.M.G. was supported by a grant from the Schweizerischer Nationalfonds zur Förderung der Wissenschaftlichen Forschung (No. 323630-164217). The work was supported by grants to L.S. from the National Institutes of Health (No. R21NS084334, No. R01AG056298), by core grant No. P30CA008748 and by a grant from Project ALS.

Author contributions

J.T. contributed to the conception, study design, data analysis and interpretation, writing of the manuscript, bioinformatics, development and execution of directed differentiation strategies from hPSCs, generation of LTNSCs, cell cycle analysis and calcium imaging. E.L.C. contributed to maintenance of hPSCs and directed differentiation of spinal cord progenitors. S.R.G. contributed to cell cycle analysis and astrocyte activation assays. E.M.G.contributed to transplantation studies and data analysis. K.A.A. and P.A.G. contributed to electrophysiology and assessment of neuronal maturation. J.A.S. contributed to generation of LTNSCs and calcium imaging. L.S. contributed to the conception, study design, data analysis and interpretation and writing of the manuscript.

Competing interests

The Memorial Sloan-Kettering Cancer Center has filed a patent application (WO2018175574A1) on the methods described in the manuscript. L.S. is the scientific cofounder of Bluerock Therapeutics.

Additional information

Supplementary information is available for this paper at https://doi.org/10.1038/s41587-019-0035-0.

Reprints and permissions information is available at www.nature.com/reprints.

Correspondence and requests for materials should be addressed to J.T. or L.S.

Publisher's note: Springer Nature remains neutral with regard to jurisdictional claims in published maps and institutional affiliations.

Methods

Cell culture. Human pluripotent stem cells (both embryonic and induced) were maintained on vitronectin-coated dishes in Essential 8 (E8) medium (Thermo) as previously described[52]. Induced PSCs were purchased from Coriell, Patient-normal lines Nos. 41865, 41866 and patient-ALS (A4V) lines Nos 35659, 35673 and 35677. Cells were used for differentiation between passages 30–50 and passaged twice every week. Cells were subjected to mycoplasma testing every 2–3 months.

Neural stem cells, LTNSCs and glial progenitors were maintained on poly-L-ornithine/laminin/fibronectin-coated dishes in NSC medium consisting of N2 media with 10 ng ml^{-1} Fibroblast growth factor 2 (FGF2), 10 ng ml^{-1} epidermal growth factor (EGF) and 1:1,000 B27 supplement. LTNSCs were used between passages 15–20 and passaged every week.

Human pluripotent stem cell-derived astrocytes were maintained on poly-L-ornithine/laminin/fibronectin-coated dishes in astrocyte media consisting of N2 medium with 10 ng ml^{-1} of HB-EGF (R&D Systems, No. 259-HE). After sorting, CD44-positive cells were passaged every week for 4 weeks and then every other week or until astrocyte processes started to detach.

Commercial fetal astrocytes (Sciencell) were initially maintained in a commercial medium containing serum (Sciencell). The serum-containing medium was switched to N2 with 10 ng ml^{-1} of HB-EGF for at least two passages before experiments were performed.

Human pluripotent stem cell-derived cortical excitatory neurons were maintained on poly-L-ornithine/laminin/fibronectin-coated dishes in neurobasal medium with brain-derived neurotrophic factor (BDNF), ascorbic acid, glial cell line-derived neurotrophic factor (GDNF) and cyclic adenosine monophosphate. More than 50% of the medium was changed every week.

Differentiation of hPSCs towards dorsal forebrain NSCs. *Dorsal forebrain patterning.* Human PSCs were dissociated into single cells, and 2.5–3.0 × 10^5 cells per cm^2 were plated onto Matrigel (BD Biosciences)-coated dishes in E8 containing 10 µM ROCK inhibitor (No. Y-27632). The following day (day 0), the cells were switched to Essential 6 (E6) medium containing 100 nM LDN193189 (LDN, Stemgent) and 10 µM SB431542 (SB, Tocris; LSB). The medium was changed every day for nine additional days (d8) as previously described[52]. To better promote an anterior forebrain fate (that is, for iPSCs), we added 2 µM of XAV939 (Stemgent) in addition to LSB for 3 days (d0–2) then from d3–8 maintained the cells in LSB without XAV939.

Generation of cortical rosettes/NSCs. From d8, the cells are dissociated with Accutase for 30 min at 37 °C and passed through a 40 µm cell strainer. The cells were resuspended in N2 medium with brain-derived neurotrophic factor (BDNF), ascorbic acid, Sonic Hedgehog (SHH) and fibroblast growth factor 8 (FGF8) (N2-BASF), and plated at 5 × 10^5 cells on air-dried poly-L-ornithine/laminin/fibronectin-coated plates in 20 µl droplets. The droplets were incubated at 37 °C for 15–20 min. N2-BASF8 medium + 10 µM ROCKi medium was overlaid on the droplets and the medium changed every day. Rosette formation was expected within 2–3 days (d12).

Following rosette formation, cells were dissociated with Accutase and replated at relatively high density (3.5 × 10^5 cells per cm^2) to prevent spontaneous differentiation. Cultured cells were assayed for correct regional patterning, differentiated or frozen.

Neuro-ectodermal differentiation of hPSCs towards ventral spinal cord. Similar to the dorsal forebrain, 2.5–3.0 × 10^5 cells per cm^2 were plated onto Matrigel (BD Biosciences)-coated dishes in hPSC knockout serum replacement (KSR)-based medium containing 10 µM ROCK inhibitor and 10 ng ml^{-1} FGF2. The following day (day 0), the cells were switched from a progressive gradient of KSR to N2 medium containing 100 nM LDN193189 and 10 µM SB431542 (LSB). The following day (day 1), the medium was switched to LSB with 1 µM of retinoic acid and 1 µM of purmorphamine and maintained for an additional 11 days (d12).

Spinal cord progenitors were dissociated with Accutase for 30 min at 37 °C and passed through a 40 µm cell strainer. The cells were then replated at 2.5 × 10^5 cells per cm^2 on poly-L-ornithine/laminin/fibronectin-coated plates and assayed for correct regional patterning, differentiated or frozen.

Derivation of LTNSCs from hPSCs. Initially, hPSCs were differentiated using the method employed for dorsal forebrain NSCs. After initial regional patterning, differentiated cells were dissociated using 10% dispase for 10 min. Cells were then separated into clumps and resuspended in N2 medium containing 20 ng ml^{-1} FGF2 and cultured in sterile, non-tissue culture-treated dishes. Cells were expected to form a high number of neurospheres, and by 3–5 days neural rosette formation within the spheres should be apparent. Having purified the neurosphere cultures, they were landed on poly-L-ornithine/laminin/fibronectin-coated plates and cultured in N2 with 10 ng ml^{-1} FGF2, 10 ng ml^{-1} EGF and 1:1,000 B27 supplement (NSC media). Rosette-stage NSC outgrowth was observed to confluency and then passaged at high density (approximately 1:3) over 2–3 months. Cells maintaining neuroepithelial morphology by passage 10 in NSC media were kept and analyzed for early NSC markers and differentiation potential.

Generation of NFIA- and SOX9-inducible constructs and lentiviral production and infection. *NFIA* and *SOX9* were cloned from cDNA using hPSC-derived astroglial progenitors (d90). FUW-tetO-GFP (Addgene, No. 30130) was digested with the restriction enzyme EcoRI to remove the GFP fragment, and either *NFIA* or *SOX9* was inserted using traditional ligation cloning. Plasmids containing *NFIA*, *SOX9*, FUCCI-O or M2-rtTA (Addgene, No. 20342), the packaging vector psPAX2 (Addgene, No. 12260) and the envelope pMD2.G (Addgene, No. 12259) were transfected into 293 T cells X-tremeGene HP (Sigma) at a molar ratio of 1:2:1. Virus was harvested at 48 and 72 h post-transfection and concentrated using AMICON Ultra-15 Centrifugal Filter Units (Millipore). NSCs were plated at 3.5 × 10^5 cells per cm^2 on poly-L-ornithine/laminin/fibronectin-coated dishes. The cells were incubated with viral particles generated (as described above) for 16–20 h. The medium was then switched to NSC medium with 1–2 µg ml^{-1} doxycycline and daily medium change for a minimum of 5 days. Cells were then detached using 0.05% trypsin and washed several times in preparation for CD44 labeling.

Intracellular FACS analysis and sorting. For both live and fixed sorting, cells were dissociated using 0.05% trypsin and washed twice with phosphate buffered saline (PBS).

Fixed GFAP and CD44 analysis. Using the BD Cytofix/Cyto Perm kit (BD), 1 × 10^6 cells were resuspended in 1 ml Cytofix and placed on ice for 1 h. The cells were then washed twice with 1× Cyto Perm Buffer and resuspended in 100 µl of 1× Cyto Perm Buffer. Alexa 647-conjugated CD44 (Biolegend) and unconjugated GFAP (Dako) were added to the cells, as described by the manufacturer, and incubated for 40 min on ice. The cells were then washed twice with 1× Cyto Perm Buffer and resuspended in 100 µl of 1× Cyto Perm Buffer for secondary labeling. For labeling of GFAP, Alexa 488 or 555 was added to the cells for 30 min on ice. Cells were washed twice with 1× Cyto Perm Buffer and submitted for analysis.

Live CD44 sorting. Approximately 4–5 × 10^6 cells were resuspended in 100 µl of sort buffer (2% fetal bovine serum, 1 mM EDTA in PBS), and CD44 conjugated with Alexa 647 was incubated, as per the manufacturer's instructions, on ice for 20–30 min. Cells were washed twice with sort buffer and submitted to the sorter. CD44-positive cells were maintained in astrocyte induction medium (N2 with 10 ng ml^{-1} heparin-bound EGF (R&D Systems) and 10 ng ml^{-1} leukemia inhibitory factor (Peprotech) without doxycycline.

Immunohistochemistry. Cells were fixed in PBS containing 4% paraformaldehyde for 10 min, permeabilized using PBS with 0.5% Triton-X for 5 min and stored in PBS with 0.2% Tween-20. The blocking solution contained 5% donkey serum in PBS with 0.2% Tween-20. Primary antibodies were diluted in the blocking solution and typically incubated overnight at 4 C. Secondary antibodies conjugated to either Alexa 488, Alexa 555 or Alexa 647 (Thermo) were added to the cells with incubation for 30 min. Nuclei were identified by staining the cells with 4′,6-diamidino-2-phenylindole (DAPI, Thermo). A list of antibodies used in this study is given in Supplementary Table 3.

Immunoblot. Cells were harvested and lysed with RIPA buffer, and protein was quantified using Precision Red (Cytoskeleton, Inc). Ten micrograms of protein was loaded to analyze protein expression. Full scans of blots for Fig. 2b (Supplementary Fig. 22), Fig. 4f (Supplementary Fig. 23), Fig. 4k (Supplementary Fig. 24) and Supplementary Fig. 7c (Supplementary Fig. 25) are available.

Gene expression and ATAC-sequencing analysis. *RNA sequencing.* RNA was isolated as previously described. Total RNA was submitted to the Memorial Sloan Kettering Cancer Center (MSKCC) Genomics Core for paired-end sequencing, aiming for 30–40 million reads. Raw FASTQ files were trimmed for adapters and aligned to the ENSEMBL GRCh38 genome build using STAR 2.5.0. Matrices were generated from the aligned files using HTSeq[53] and imported into DESeq2[54] for further analysis using a standard pipeline. A list of the normalized read counts represented in Fig. 1 and Supplementary Fig. 8 can be found in Supplementary Table 1, and a list of genes expressed from all samples in Fig. 4 can be found in Supplementary Table 2.

ATAC sequencing. Raw FASTQ files were aligned to the hg19 genome build using Bowtie2[55]. Comparative analysis of alignment files was performed using the deepTools software package[56]. Motif analysis and peak annotation were performed using HOMER software[57] and visualized using the IGV browser[58].

All FASTQ files and Supplementary files were uploaded to National Center for Biotechnology Information Gene Expression Omnibus under accession code GSE104232.

Cytokine treatment of human astrocytes. Astrocytes were plated at 2 × 10^4 cells per cm^2 and treated with 3 ng ml^{-1} IL-1α (Sigma), 30 ng ml^{-1} tumor necrosis factor (Cell Signaling Tech) and 400 ng ml^{-1} C1q (MyBioSource) for 24 h. The medium was isolated and spun down to remove debris, and C3 levels were measured using the Human Complement C3 ELISA Kit (Abcam) as per the manufacturer's instructions.

Cell cycle analysis. Cells with dissociated nuclei were isolated using resuspension buffer (10 mM Tris-HCl, 30 mM NaCl, 20 mM $MgCl_2$) and subsequently the resuspension buffer with 1% NP-40 for cell cycle analysis. Propidium iodine (250 ng ml^{-1}) was added to the cells followed by analysis with FACS. A minimum of 10,000 events were analyzed per condition. Data acquired were imported and analyzed by Flowjo software.

Transplantation of NSCs, glial precursors and astrocytes into adult cortex. All surgeries were performed according to National Institutes of Health guidelines and were approved by the local Institutional Animal Care and Use Committee, the Institutional Biosafety Committee and the Embryonic Stem Cell Research Committee. A total of eight (or 20) [CF1] NOD-SCID IL2-Rgc null mice (20–35 g; Jackson Laboratory) received cell transplantation. Mice were anesthetized with isoflurane 5% at a maintenance flow rate of 2–3%. A total of 7×10^4 NFIA-induced astrocytes in 2 µl were transplanted through a 5 µl Hamilton syringe at a rate of 1 µl min^{-1} by an infusion pump attached to a stereotactic micromanipulator, into the genu of the corpus callosum (coordinates: AP +0.740, ML −1.00, DV −2.30 from bregma). A total of 2×10^5 LTNSC 2 µl^{-1} were transplanted into the subcortical gray matter, striatum (coordinates AP +0.500, ML −1.90, DV −3.20 from bregma). A total of 7.5×10^4 H1-GFP-derived astrocytes in 2 µl were transplanted into the genu of the corpus callosum (coordinates: AP +0.740, ML −1.00, DV −2.30 from bregma). The mice were sacrificed at 1, 6 and 12 weeks after transplantation for immunohistochemical analysis.

Tissue processing. Mice were euthanized with an overdose of pentobarbital given intraperitoneally, then transcardially perfused with PBS followed by paraformaldehyde 4%. Brains were removed after gentle dissection, maintained overnight in 4% paraformaldehyde then soaked in 30% sucrose for 2–3 days. Brain coronal sectioning (30 µm at −20 °C) was performed by cryostat after embedding with Optimal Cutting Temperature (OCT) (Sakura Finetek).

Calcium imaging. Human pluripotent stem cell-derived neural stem cells, astrocytes or primary astrocytes (Sciencell) were plated onto poly-L-ornithine/laminin/fibronectin-coated 0.5 mm black ΔT dishes (Bioptechs) and used for calcium imaging as previously described[59] between days 60 and 120. Cultures were incubated with 5 µM Fura-2 (Thermo) for 30 min at 37 C and dishes were mounted on a ΔT Heated Lid w/Perfusion system (Bioptechs). Cultures were perfused with normal Tyrode's solution (pH 7.4) containing 125 mM NaCl, 5 mM KCl, 25 mM glucose, 25 mM HEPES, 1 mM $MgCl_2$, 2 mM $CaCl_2$ and 0.1% (w/v) bovine serum albumin. Cultures were supplemented with glutamate (100 µM), ATP (30 µM) or KCl (65 mM) for 1 min and imaged every 30 s at 340 and 380 nm at a minimum of seven positions. Time-lapse images were analyzed using FIJI (ImageJ) by calculating the signal ratio between 380 and 340 nm.

Glutamate excitotoxicity assay. Cortical neurons were derived by differentiating hPSCs towards a neuro-ectodermal fate (see above). Neuro-ectodermal cells were then dissociated and replated to generate neural rosettes, and further differentiated into neurons by treatment with 10 µM of a γ-secretase inhibitor (DAPT). Neurons were then replated and assayed for maturation markers or glutamate excitotoxicity[60] with or without astrocytes. For glutamate excitotoxicity studies, 100,000 neurons per cm^2 were plated on poly-L-ornithine/laminin/fibronectin dishes in N2 medium with BDNF, ascorbic acid and GDNF. NFIA-induced astrocytes were added at 150,000 cells per cm^2 and co-cultured for an additional 5 days. Cells were then treated with 100 or 500 µm (final) L-glutamate for 1 h in Hanks' buffered salt solution and recovered in N2 medium with BDNF, ascorbic acid and GDNF. Resazurin was added 48 h after glutamate treatment to determine cell viability.

Bisulfite conversion and sequencing. LTNSCs infected with NFIA were treated with dox for 5 days and sorted for CD44. Cells were isolated and bisulfite conversion was performed using the EZ DNA Methylation-Direct Kit (Zymo) as described by the manufacturer. Primers for the regions of the GFAP STAT3 binding site were described previously[61]. Briefly, P1 and P2 correspond to −1,500 bp from the start site of GFAP (P1 forward: 5′ AGGAGGGTTGTTTGTTTTTTAGAA, P1 reverse: 5′ CCCTTCCTTATCTAACCTCCCTATA and P2 forward: 5′ GTAGATT TGGTAGTATTGGGTTGGT, P2 reverse: 5′ CCCTCACCCATTTATATCCTTAAA. The GFAP promoter region was amplified using ZymoTaq Premix (Zymo) and cloned into the TOPO Zero Blunt vector (Invitrogen). A minimum of ten colonies per condition were sent for sequencing.

Electrophysiology. Whole-cell recordings were performed as described previously[62], with slight modifications. Briefly, neurons were visualized using a Zeiss microscope (Axioscope) equipped with a ×4 objective and a ×40 water immersion. Neurons were recorded at 23–24 °C. Input resistance was measured from voltage response elicited by intracellular injection of a current pulse (−100 pA, 200 ms). Membrane voltage was low-pass filtered at 5 kHz and digitized at 10 kHz, using a Multiclamp 700B amplifier connected to a DigiData 1322 A interface (Axon Instruments) using Clampex 10.2 software (Molecular Devices). Liquid junction potentials were calculated and corrected offline[63]. During recording, neurons were perfused with freshly prepared artificial cerebrospinal fluid (126 mM NaCl, 26 mM $NaHCO_3$, 3.6 mM KCl, 1.2 mM NaH_2PO_4, 1.5 mM $MgCl_2$, 2.5 mM $CaCl_2$ and 10 mM glucose), and the solution was saturated with 95% O_2–5% CO_2. Pipette solution for all recordings contained 140 mM CsCl, 10 mM NaCl, 10 mM HEPES, 0.5 mM EGTA, 3 mm Mg-ATP, 0.2 mM Na-GTP and 10 mM Na2-phosphocreatine, pH adjusted to 7.3 with CsOH. Bicuculline methochloride (20 µM, Tocris), 1 µM strychnine HCl (Sigma) and 0.5 µM tetrodotoxin (TTX, Alomone Labs) were added to the artificial cerebrospinal fluid for mEPSC recordings to block gamma-aminobutyric acid receptors, glycine receptors and Na^+ channels, respectively. Neurons were held at –80 mV and continuous recording of mEPSCs was made using Axoscope software (Molecular Devices). Data processing and analysis were performed using MiniAnalysis (Synaptosoft) and Clampfit 10 (Molecular Devices). Events were detected by setting the threshold value, followed by visual confirmation of mEPSC detection. Statistical analysis was performed using Student's *t*-test or Mann–Whitney rank sum test as necessary, with a significant difference at $P < 0.05$. Data are expressed as mean ± standard error.

Reporting Summary. Further information on research design is available in the Nature Research Reporting Summary linked to this article.

Data availability

The data and reagents in this study are available from the corresponding author upon reasonable request. All FASTQ files and Supplementary files were uploaded to National Center for Biotechnology Information Gene Expression Omnibus under accession code GSE104232.

References

52. Tchieu, J. et al. A modular platform for differentiation of human PSCs into all major ectodermal lineages. *Cell Stem Cell.* **21**, 399–410 e397 (2017).
53. Anders, S., Pyl, P. T. & Huber, W. HTSeq—a Python framework to work with high-throughput sequencing data. *Bioinformatics* **31**, 166–169 (2015).
54. Love, M. I., Huber, W. & Anders, S. Moderated estimation of fold change and dispersion for RNA-seq data with DESeq2. *Genome Biol.* **15**, 550 (2014).
55. Langmead, B. & Salzberg, S. L. Fast gapped-read alignment with Bowtie 2. *Nat. Methods* **9**, 357–359 (2012).
56. Ramirez, F. et al. deepTools2: a next generation web server for deep-sequencing data analysis. *Nucleic Acids Res.* **44**, W160–W165 (2016).
57. Heinz, S. et al. Simple combinations of lineage-determining transcription factors prime cis-regulatory elements required for macrophage and B cell identities. *Mol. Cell* **38**, 576–589 (2010).
58. Robinson, J. T. et al. Integrative genomics viewer. *Nat. Biotechnol.* **29**, 24–26 (2011).
59. Steinbeck, J. A. et al. Functional connectivity under optogenetic control allows modeling of human neuromuscular disease. *Cell Stem Cell* **18**, 134–143 (2016).
60. Chiricozzi, E. et al. Group IIA secretory phospholipase A2 (GIIA) mediates apoptotic death during NMDA receptor activation in rat primary cortical neurons. *J. Neurochem.* **112**, 1574–1583 (2010).
61. Cheng, P. Y. et al. Interplay between SIN3A and STAT3 mediates chromatin conformational changes and GFAP expression during cellular differentiation. *PLoS ONE* **6**, e22018 (2011).
62. Maroof, A. M. et al. Directed differentiation and functional maturation of cortical interneurons from human embryonic stem cells. *Cell Stem Cell* **12**, 559–572 (2013).
63. Ying, S. W. & Goldstein, P. A. Propofol suppresses synaptic responsiveness of somatosensory relay neurons to excitatory input by potentiating GABA(A) receptor chloride channels. *Mol. Pain* **1**, 2 (2005).

nature research

Corresponding author(s): Lorenz Studer

Reporting Summary

Nature Research wishes to improve the reproducibility of the work that we publish. This form provides structure for consistency and transparency in reporting. For further information on Nature Research policies, see Authors & Referees and the Editorial Policy Checklist.

Statistical parameters

When statistical analyses are reported, confirm that the following items are present in the relevant location (e.g. figure legend, table legend, main text, or Methods section).

n/a	Confirmed	
☐	☒	The exact sample size (*n*) for each experimental group/condition, given as a discrete number and unit of measurement
☐	☒	An indication of whether measurements were taken from distinct samples or whether the same sample was measured repeatedly
☐	☒	The statistical test(s) used AND whether they are one- or two-sided *Only common tests should be described solely by name; describe more complex techniques in the Methods section.*
☒	☐	A description of all covariates tested
☐	☒	A description of any assumptions or corrections, such as tests of normality and adjustment for multiple comparisons
☐	☒	A full description of the statistics including central tendency (e.g. means) or other basic estimates (e.g. regression coefficient) AND variation (e.g. standard deviation) or associated estimates of uncertainty (e.g. confidence intervals)
☐	☒	For null hypothesis testing, the test statistic (e.g. *F*, *t*, *r*) with confidence intervals, effect sizes, degrees of freedom and *P* value noted *Give P values as exact values whenever suitable.*
☒	☐	For Bayesian analysis, information on the choice of priors and Markov chain Monte Carlo settings
☒	☐	For hierarchical and complex designs, identification of the appropriate level for tests and full reporting of outcomes
☒	☐	Estimates of effect sizes (e.g. Cohen's *d*, Pearson's *r*), indicating how they were calculated
☐	☒	Clearly defined error bars *State explicitly what error bars represent (e.g. SD, SE, CI)*

Our web collection on statistics for biologists may be useful.

Software and code

Policy information about availability of computer code

Data collection	External RNA sequencing data was downloaded using the SRA Toolkit (NCBI).
Data analysis	ATAC-Seq analysis was performed following the workflow: https://www.encodeproject.org/atac-seq/ which was aligned to hg38 and uses MACS (v2.2.1) and HOMER (v4.9.1) software for peak and motif identification. The IGV browser (v2.3.97) was used to visualize peak locations. RNA-Seq analysis was performed following the workflow: https://www.bioconductor.org/help/workflows/rnaseqGene/ which was aligned to hg38 and uses Bowtie2 (v2.2.5) for alignment, HTSeq (v0.6.1p1) for generation of a counts table and DESeq2 (v1.20.0) for differential gene expression analysis. The IGV browser (v2.3.97) was used to visualize RNA sequencing mapping. The Imaris software was used to identify overlap of pre and post synaptic proteins using signal thresholding. FIJI/ImageJ (v2.0.0-rc-68) was used to analyze and quantify the calcium imaging as well as analysis of the FUCCI-O timelapse movies. Flowjo (v10.4) software was used to gate and quantify the number of cells.

For manuscripts utilizing custom algorithms or software that are central to the research but not yet described in published literature, software must be made available to editors/reviewers upon request. We strongly encourage code deposition in a community repository (e.g. GitHub). See the Nature Research guidelines for submitting code & software for further information.

Data

Policy information about availability of data

All manuscripts must include a data availability statement. This statement should provide the following information, where applicable:

- Accession codes, unique identifiers, or web links for publicly available datasets
- A list of figures that have associated raw data
- A description of any restrictions on data availability

Data generated during this study is deposited at NCBI GEO (Both ATAC-seq and RNA-seq) under accession number GSE104232.

Field-specific reporting

Please select the best fit for your research. If you are not sure, read the appropriate sections before making your selection.

☒ Life sciences ☐ Behavioural & social sciences ☐ Ecological, evolutionary & environmental sciences

For a reference copy of the document with all sections, see nature.com/authors/policies/ReportingSummary-flat.pdf

Life sciences study design

All studies must disclose on these points even when the disclosure is negative.

Sample size	A minimum of 3 independent biological replicates were analyzed for the study. The choice of 3 was the minimum in terms of reproducibility and manageable within the time frame. We believe the sample size was sufficient as our experiments were highly reproducible within those 3 experiments.
Data exclusions	hPSC differentiations where cultures did not meet the expected identity were discarded. Samples that resulted in poor RNA or protein quality were discarded. Although the exclusions were not pre-established, our goal was to trigger the gliogenic switch in neural stem cells as well as other regionally distinct neural stem cell populations. If we could not generate them for any particular reason, these differentiations would not be able to address our main question. Technically, if we could not isolate good quality and quantity of RNA or protein we could not extract information from these samples.
Replication	Aside from technical issues, the findings for NFIA-induced experiments were reproducible through a minimum of 3 biological replicates in LTNSCs. Astrocytes generated from NFIA were replicated and extended to other pluripotent stem cell lines (both ES and iPS).
Randomization	Experiments were not randomized however additional members of the laboratory have performed independent experiments using this method and have successfully generated astrocytes.
Blinding	Experiments were not blinded because we sought to investigate the role of NFIA in triggering glial competency and the results were clear where neural stem cells exposed to NFIA lead to astrocyte differentiation versus neural stem cells not exposed remain as stem cells or becomes neurons.

Reporting for specific materials, systems and methods

Materials & experimental systems

n/a	Involved in the study
☐	☒ Unique biological materials
☐	☒ Antibodies
☐	☒ Eukaryotic cell lines
☒	☐ Palaeontology
☐	☒ Animals and other organisms
☒	☐ Human research participants

Methods

n/a	Involved in the study
☒	☐ ChIP-seq
☐	☒ Flow cytometry
☒	☐ MRI-based neuroimaging

Unique biological materials

Policy information about availability of materials

Obtaining unique materials

There are no restrictions on availability of materials as the majority were commercial. Our unique reagent (FUW-NFIA, FUW-SOX9) will be submitted to Addgene.

Antibodies

Antibodies used

Antigen Supplier Catalog Number Host Species Clone name Assay dilution
NFIA Sigma HPA006111 Rabbit Polyclonal Immunofluorescence 1:500
GFAP Biolegend 829401 Chicken Polyclonal Immunofluorescence 1:1000
GFAP Dako Z033429-2 Rabbit Polyclonal Immunofluorescence 1:1000
GFP Abcam ab13970 Chicken Polyclonal Immunofluorescence 1:1000
SLC1A2 Abcam ab416 Rabbit Polyclonal Immunofluorescence 1:1000
SYN1 Sigma S193 Rabbit Polyclonal Immunofluorescence and Western Blot 1:250
MUNC13.1 Synaptic Systems 126103 Rabbit Polyclonal Western Blot 1:1000
human cytoplasm Takara "Y40410 " Mouse unknown Immunofluorescence 1:500
human GFAP Takara Y40420 Mouse unknown Immunofluorescence 1:500
TUJ1 R&D MAB1195 Mouse TuJ-1 Immunofluorescence 1:1000
CCNA1 Santa Cruz sc-271645 Goat Polyclonal Western Blot 1:1000
CDKN1A Thermo MA5-14949 Mouse R.229.6 Western Blot 1:1000
GAPDH Fitzgerald 10R-G109A Mouse 6C5 Western Blot 1:10000
POU5F1/OCT4 Cell Signaling Technology 2750S Rabbit Polyclonal Immunofluorescence 1:250
SOX2 Biolegend 630802 Rabbit Polyclonal Immunofluorescence 1:250
PLZF R&D MAB2944 Mouse 6318100 Immunofluorescence 1:250
AQP4 Santa Cruz "sc-9888 " Goat Polyclonal Immunofluorescence 1:100
MAP2 Sigma M1406 Mouse AP-20 Immunofluorescence 1:250
NESTIN Neuromics "MO15012 " Mouse 196908 Immunofluorescence 1:500
OTX2 Neuromics GT15095 Goat Polyclonal Immunofluorescence 1:500
FOXG1 Neuracell NCFAB Rabbit Polyclonal Immunofluorescence 1:500
ZO-1 BD Biosciences 610966 Mouse 1/ZO-1 Immunofluorescence 1:500
CD44 Cell Signaling Technology 3570 Mouse 156-3C11 Immunofluorescence 1:500
CD44 Biolegend 103018 Mouse IM7 FACS 1:500
HOMER1 Synaptic Systems 160 011 Mouse unknown Immunofluorescence 1:100
HOXB4 DSHB I12 anti-Hoxb4 Mouse unknown Immunofluorescence 1:100

Validation

Antigen Validated by Manufacturer
NFIA human validated
GFAP human validated
GFAP human validated
GFP yes
SLC1A2 human validated
SYN1 human validated
MUNC13.1 human validated
human cytoplasm human validated
human GFAP human validated
TUJ1 human validated
CCNA1 human validated
CDKN1A human validated
GAPDH human validated
POU5F1/OCT4 human validated
SOX2 human validated
PLZF human validated
AQP4 tested in mouse
MAP2 human validated
NESTIN human validated
OTX2 human validated
FOXG1 human validated
ZO-1 human validated
CD44 human validated
CD44 human validated
HOMER1 human validated
HOXB4 human validated

Eukaryotic cell lines

Policy information about cell lines

Cell line source(s)

H9 (WA-09), H1(WA-01) from the University of Wisconsin, Madison. MEL1 from University of Queensland. 41865-iPSC

Cell line source(s)	("WT1"), 35659-iPSC ("ALS1"), 35673-iPSC ("ALS2"). Additional iPSCs 41866-iPSC ("WT2") and 35677-iPSC ("ALS3") were obtained from Coriell.
Authentication	hESCs were cell line authenticated by STR, the iPSC lines were not.
Mycoplasma contamination	All cell lines are regularly tested for mycoplasma and are negative.
Commonly misidentified lines (See ICLAC register)	No commonly misidentified lines are used in this study.

Animals and other organisms

Policy information about studies involving animals; ARRIVE guidelines recommended for reporting animal research

Laboratory animals	Mus musculus, NOD.Cg-Prkdc<scid>Il2rg<tm1Wjl>/SzJ both female and male. Age of mice: 6-8 weeks.
Wild animals	None.
Field-collected samples	None.

Flow Cytometry

Plots

Confirm that:

☒ The axis labels state the marker and fluorochrome used (e.g. CD4-FITC).

☒ The axis scales are clearly visible. Include numbers along axes only for bottom left plot of group (a 'group' is an analysis of identical markers).

☒ All plots are contour plots with outliers or pseudocolor plots.

☒ A numerical value for number of cells or percentage (with statistics) is provided.

Methodology

Sample preparation	See Flow Report document
Instrument	See Flow Report document
Software	See Flow Report document
Cell population abundance	See Flow Report document
Gating strategy	See Flow Report document

☒ Tick this box to confirm that a figure exemplifying the gating strategy is provided in the Supplementary Information.

nature research

Corresponding author(s): Lorenz Studer

Flow Cytometry Reporting Summary

Form fields will expand as needed. Please do not leave fields blank.

Data presentation

For all flow cytometry data, confirm that:

☒ 1. The axis labels state the marker and fluorochrome used (e.g. CD4-FITC).

☒ 2. The axis scales are clearly visible. Include numbers along axes only for bottom left plot of group (a 'group' is an analysis of identical markers).

☒ 3. All plots are contour plots with outliers or pseudocolor plots.

☒ 4. A numerical value for number of cells or percentage (with statistics) is provided.

Methodological details

5. Describe the sample preparation.	For live sorts: samples were dissociated with 0.5% Trypsin, inactivated with media containing 10% serum and resuspended in sort buffer (PBS, 2% fetal bovine serum, 1mM EDTA). Primary antibodies (CD44-A647-conjugated) For intracellular FACS analysis: Samples were dissociated with 0.5% Trypsin, inactivated with media containing 10% serum and washed 2 times with PBS. Samples were fixed in the CytoFix solution (BD) for 1 hour on ice. After fixation, cells were washed 3 times with PBS and stored at 4 degree. For cell cycle analysis: Samples were dissociated with 0.5% Trypsin, inactivated with media containing 10% serum and washed 2 times with PBS. Nuclei were then isolated.
6. Identify the instrument used for data collection.	Samples were sorted using the FACS Aria IIu (BD). Analysis were performed on either the LSRII or Fortessa 3 (BD).
7. Describe the software used to collect and analyze the flow cytometry data.	The software used to collect data was FACS Diva and the subsequent analysis of the .fcs files were performed using Flowjo 10.
8. Describe the abundance of the relevant cell populations within post-sort fractions.	CD44 positive cell fractions underwent post sort analysis and was found to have > 95% purity.
9. Describe the gating strategy used.	The gating strategy is as follows: 1. Cells are filtered for debris using SSC-A/FSC-A 2. Cells are then filtered by SSC-W/SSC-H to isolate singlets 3. For live sorts, cells had to be DAPI negative 4. Neurogenic neural stem cells (for example, CD44 negative) are used as a control for CD44 positive sorting.

Tick this box to confirm that a figure exemplifying the gating strategy is provided in the Supplementary Information. ☒